https://doi.org/10.5194/gmd-2020-435
Preprint. Discussion started: 31 March 2021

Geoscientific Model Development Discussions
Open Access
EGU

Non-Hydrostatic RegCM4 (RegCM4-NH): Model description and case studies over multiple domains

Coppola Erika[1], Stocchi Paolo[2], Pichelli Emanuela[1], Torres Alavez Jose Abraham[1], Glazer Russell[1], Giuliani Graziano[1], Di Sante Fabio[1], Nogherotto Rita[1], Giorgi Filippo [1]

1. International Centre for Theoretical Physics (ICTP),Trieste, Italy
2. Institute of Atmospheric Sciences and Climate, National Research Council of Italy, CNR-ISAC, Bologna, Italy

Correspondence to: Erika Coppola (coppolae@ictp.it)

Abstract. We describe the development of a non-hydrostatic version of the regional climate model RegCM4, called RegCM4-NH, for use at convection-permitting resolutions. The non-hydrostatic dynamical core of the Mesoscale Model MM5 is introduced in the RegCM4, with some modifications to increase stability and applicability of the model to long-term climate simulations. Newly available explicit microphysics schemes are also described, and three case studies of intense convection events are carried out in order to illustrate the performance of the model. They are all run at convection-permitting grid spacing of 3 km over domains in northern California, Texas and the Lake Victoria region, without the use of parameterized cumulus convection. A substantial improvement is found in the simulations compared to corresponding coarser resolution (12 km) runs completed with the hydrostatic version of the model employing parameterized convection. RegCM4-NH is currently being used in different projects for regional climate simulations at convection permitting resolutions, and is intended to be a resource for users of the RegCM modeling system.

1 Introduction

Since the pioneering work of Dickinson et al. (1989) and Giorgi and Bates (1989), the dynamical downscaling technique based on limited area Regional Climate Models (RCMs) has been widely used worldwide, and a number of RCM systems have been developed (Giorgi 2019). One of these systems, and in fact the first one to be developed, is the RegCM. The first version of RegCM, named RegCM1, was produced by Dickinson et al. (1989) and Giorgi and Bates (1989) as a development of the Mesoscale Model version 4 (MM4) (Anthes et al, 1987) of the National Center for Atmospheric Research (NCAR). This was followed by further model versions: RegCM2 (Giorgi et al. 1993a,b), RegCM2.5, (Giorgi and Mearns 1999), RegCM3 (Pal et al. 2007), and lastly RegCM4 (Giorgi et al 2012). Except for the passage from RegCM1 to RegCM2, in which the model dynamical core was updated from that of the MM4 to that of the MM5 (Grell et al. 1995), these model evolutions were mostly based on additions of new and more advanced physics packages. In particular, RegCM4 is today used by a large community for numerous projects and applications, from process studies to paleo and future climate projections, including participation to the Coordinated Regional Downscaling EXperiment (CORDEX, Giorgi et al. 2009; Gutowski et al. 2016). The model can also be coupled with ocean, land and chemistry/aerosol modules in a fully interactive way (Sitz et al. 2017).

https://doi.org/10.5194/gmd-2020-435
Preprint. Discussion started: 31 March 2021

The dynamical core of the standard version of RegCM4 is hydrostatic, with sigma-p vertical coordinates. As a result, the model can be effectively run for grid spacings of ~10 km or more, for which the hydrostatic assumption is valid. However, the RCM community is rapidly moving to higher resolutions of a few km, named "convection-permitting" (Prein et al. 2015; Coppola et al. 2020) and therefore the dynamical core of RegCM4 has been upgraded to include a non-hydrostatic dynamics representation usable for very high resolution applications. This upgrade, which we name RegCM4-NH, is essentially based on the implementation of the MM5 non-hydrostatic dynamical core within the RegCM4 framework, which has an entirely different set of model physics compared to MM5.
Long term simulations carried out through the new generation RegCM4-NH contribute to some broad project dedicated to the study of climate at the convection km-scale: namely the European Climate Prediction System (EUCP, Hewitt and Lowe 2018) and the CORDEX Flagship Pilot Study dedicated to convection (CORDEX-FPSCONV, Coppola et al. 2020), and it is starting to be used more broadly by the RegCM modeling community.
The recent papers by Ban et al. (2021) and Pichelli et al. (2021) document results of the first multi-model experiment of 10-year simulations at the convection-permitting scale over the so-called great alpine region. Two different simulations over the present days contribute to the evaluation analysis for precipitation (Ban et al., 2021), respectively carried out by the research group of the International Centre for Theoretical Physics (ICTP) and the Croatian Meteorological and Hydrological Service (DHMZ) with two different physical configurations. The results show that REGCM-NH simulations largely reduce the bias with observations when going from coarse to higher resolution, contributing to adding value to the representation of rainfall. Pichelli et al. (2021) present the multi-model ensemble simulations driven by selected CMIP5 GCM projections over decades 1996–2005 and 2090–2099 under the rcp8.5 scenario. ICTP contributed to the experiment with simulations performed by the new RegCM-NH core driven by the MOCH-HadGEM GCM (r1i1p1) in a two level nest configuration (respectively at 12 and 3 km grid). The paper shows new insights into future changes, with, among the others, summer and autumn hourly rainfall intensification more than previously documented by coarser resolution model experiments, as well as an increase of high-impact weather events frequency.

In this paper we describe the structure of RegCM4-NH and provide some illustrative examples of its performance, so that model users can have a basic reference providing them with background information on the model. In the next section we first describe the new model dynamical core, while the illustrative applications are presented in section 4. Section 5 finally provides some discussion of future developments planned for the RegCM system.

2 Model description

In the development of RegCM4-NH, the RegCM4 as described by Giorgi et al. (2012) was modified to include, as an additional option selectable through a switch, the non-hydrostatic dynamical core (*idynamic* = 2 namelist option as described in RegCM-4.7.1/Doc/README.namelist of the source code) of the mesoscale model MM5 (Grell et al. 1995), which uses the equations described by Grell et al. (1995). This dynamical core was selected because it follows the same grid and variable structure of the RegCM4, which substantially facilitated its implementation (Elguindi et al. 2017).

https://doi.org/10.5194/gmd-2020-435
Preprint. Discussion started: 31 March 2021

Geoscientific Model Development Discussions

The model equations with complete description of the Coriolis force and a top radiative boundary condition, along with the finite differencing scheme, are given in Grell et al. (1995). Pressure, p, temperature, T, and density, , are first decomposed into a standard prescribed reference vertical profile plus a time varying perturbation. The prognostic equations are then calculated using the pressure perturbation values. Compared to the original MM5 dynamical core, the following modifications were implemented in order to achieve increased stability for long term climate simulations (Elguindi et al. 2017 document any modifications which follow the choice of the non-hydrostatic dynamical core through the namelist parameter *idynamic* = 2; further available user-dependant options, and the corresponding section in the namelist, are explicitly indicated):

i) The reference state surface temperature profile is computed using a latitude dependent climatological temperature distribution and thus is a function of the specific domain coordinates (*base_state_pressure*, *logp_lrate* parameters in *&referenceatm*) (Elguindi et al. 2017);

ii) The lateral time dependent boundary conditions (*iboudy* in *&physicsparam*) for each prognostic variable use the same exponential relaxation technique (*iboudy* = 5) described in Giorgi et al. (1993). The linear MM5 relaxation scheme is kept only as an option (*iboudy* = 1);

iii) The advection term in the model equations, which in the MM5 code is implemented using a centered finite difference approach, was changed to include a greater upstream weight factor as a function of the local Courant number (Elguindi et al. 2017). The maximum value of the weight factor is user configurable (*uoffc* in *&dynparam*);

iv) The moisture term uses the same advection scheme as the other variables (Elguindi et al. 2017) and not a complete upstream scheme as in the MM5 code (Grell et al. 1995);

v) A local flux limiter reduces the advection terms to remove unrealistic strong gradients and its limits are user configurable (in *&dynparam* section the maximum gradient fraction for advection to stop for: temperature, *t_extrema*, specific humidity, *q_rel_extrema*, liquid cloud content, *c_rel_extrema* and for tracers, *t_rel_extrema*);

vi) The diffusion stencil of the Laplace equation uses a nine point approach as in LeVeque (2006) and a topography dependent environmental diffusion coefficient is used (Elguindi et al. 2017) as in the hydrostatic version of the code (Giorgi et al. 1993b);

vii) The top boundary radiative condition (*ifupr* = 1 in *&nonhydroparam*) adopted in the semi-implicit vertical differencing scheme to reduce the reflection of energy waves uses coefficients on a 13x13 matrix which are re-computed every simulation day and not kept constant throughout the whole simulation as in the MM5 code;

https://doi.org/10.5194/gmd-2020-435
Preprint. Discussion started: 31 March 2021

Geoscientific Model Development
Discussions

viii) The dynamical control parameter β in the semi-implicit vertical differencing scheme (*nhbet* in *&nonhydroparam*) is used for acoustic wave damping (Elguindi et al. 2017) and is user configurable (Klemp and Dudhia, 2008);

ix) A Rayleigh damping (ifrayd = 1 in &nonhydroparam) of the status variables towards the input GCM boundary conditions can be activated in the top layers (*rayndamp* configuring the number of top levels to apply) with a configurable relaxation time (*rayalpha0*, Klemp and Lilly, 1978, Durran and Klemp, 1983);

x) The water species time filtering uses the Williams (2009) modified filter with α = 0.53 instead of the RA filter used by all the other variables. The ν factor in the RA filter is user configurable (*gnu1* and *gnu2* in *&dynparam*).

With these modifications, the model basic equations (same as in the MM5) are (Elguindi et al. 2017) :

$$\frac{\partial p^* u}{\partial t} = -m^2\left[\frac{\partial p^* uu/m}{\partial x} + \frac{\partial p^* vu/m}{\partial y}\right] - \frac{\partial p^* u\dot{\sigma}}{\partial \sigma} + uDIV - \frac{mp^*}{\rho}\left[\frac{\partial p'}{\partial x} - \frac{\sigma}{p^*}\frac{\partial p^*}{\partial x}\frac{\partial p'}{\partial \sigma}\right] + p^* fv - p^* ew\cos\theta + D_u \quad (1)$$

$$\frac{\partial p^* v}{\partial t} = -m^2\left[\frac{\partial p^* uv/m}{\partial x} + \frac{\partial p^* vv/m}{\partial y}\right] - \frac{\partial p^* v\dot{\sigma}}{\partial \sigma} + vDIV - \frac{mp^*}{\rho}\left[\frac{\partial p'}{\partial y} - \frac{\sigma}{p^*}\frac{\partial p^*}{\partial y}\frac{\partial p'}{\partial \sigma}\right] - p^* fu + p^* ew\sin\theta + D_v \quad (2)$$

$$\frac{\partial p^* w}{\partial t} = -m^2\left[\frac{\partial p^* uw/m}{\partial x} + \frac{\partial p^* vw/m}{\partial y}\right] - \frac{\partial p^* w\dot{\sigma}}{\partial \sigma} + wDIV + p^* g\frac{\rho_0}{\rho}\left[\frac{1}{p^*}\frac{\partial p'}{\partial \sigma} + \frac{T_v'}{T} - \frac{T_0 p'}{T p_0}\right] - p^* g\left[(q_c + q_r)\right] + p^* e\left(u\cos\theta - v\sin\theta\right) + D_w \quad (3)$$

$$\frac{\partial p^* p'}{\partial t} = -m^2\left[\frac{\partial p^* up'/m}{\partial x} + \frac{\partial p^* vp'/m}{\partial y}\right] - \frac{\partial p^* p'\dot{\sigma}}{\partial \sigma} + p' DIV - m^2 p^* \gamma p\left[\frac{\partial u/m}{\partial x} - \frac{\sigma}{mp^*}\frac{\partial p^*}{\partial x}\frac{\partial u}{\partial \sigma} + \frac{\partial v/m}{\partial y} - \frac{\sigma}{mp^*}\frac{\partial p^*}{\partial y}\frac{\partial v}{\partial \sigma}\right] + \rho_0 g\gamma p\frac{\partial w}{\partial \sigma} + p^* \rho_0 g \quad (4)$$

$$\frac{\partial p^* T}{\partial t} = -m^2\left[\frac{\partial p^* uT/m}{\partial x} + \frac{\partial p^* vT/m}{\partial y}\right] - \frac{\partial p^* T\dot{\sigma}}{\partial \sigma} + TDIV + \frac{1}{\rho c_p}\left[p^*\frac{Dp'}{Dt} - \rho_0 g p^* w - D_{p'}\right] + p^*\frac{\dot{Q}}{c_p} + D_T \quad (5)$$

https://doi.org/10.5194/gmd-2020-435
Preprint. Discussion started: 31 March 2021

Geoscientific Model Development Discussions

Where:

$$DIV = m^2 \left[\frac{\partial p^* u/m}{\partial x} + \frac{\partial p^* v/m}{\partial y} \right] + \frac{\partial p^* \dot{\sigma}}{\partial \sigma}$$

$$\dot{\sigma} = -\frac{\rho_0 g}{p^*} w - \frac{m\sigma}{p^*} \frac{\partial p^*}{\partial x} u - \frac{m\sigma}{p^*} \frac{\partial p^*}{\partial y} v$$

$$\tan\theta = -\cos\phi \frac{\partial \lambda / \partial y}{\partial \phi / \partial x}$$

$$p(x,y,z,t) = p_0(z) + p'(x,y,z,t)$$
$$T(x,y,z,t) = T_0(z) + T'(x,y,z,t)$$
$$\rho(x,y,z,t) = \rho_0(z) + \rho'(x,y,z,t)$$

and the vertical sigma coordinate is defined as:

$$\sigma = \frac{(p_0 - p_t)}{(p_s - p_t)}$$

where p_s is the surface pressure and p_0 is the reference pressure profile. The total pressure at each grid point is thus given as:

$$p(x,y,z,t) = p^* \sigma(k) + p_t + p'(x,y,z,t)$$

With p_t being the top model pressure assuming a fixed rigid lid.

The model physics schemes for boundary layer, radiative transfer, land and ocean surface processes, cloud and precipitation processes are extensively described in Giorgi et al. (2012) and references therein. For each physics component a number of parameterization options are available, and can be selected using a switch selected by the user. As mentioned, the use of non-hydrostatic dynamics is especially important when going to convection-permitting resolutions of a few km (Prein et al. 2015). At these resolutions the scale separation assumption underlying the use of cumulus convection schemes is not valid any more, and explicit cloud microphysics representations are necessary. The RegCM4 model currently includes two newly implemented microphysics schemes, the Nogherotto-Tompkins (Nogherotto et al. 2016) and the WSM5 scheme from the Weather Research Forecast (WRF, Skamarok et al. 2008) model, which are briefly described in the next sections for information to model users.

2.1 Explicit microphysics schemes

https://doi.org/10.5194/gmd-2020-435
Preprint. Discussion started: 31 March 2021

2.1.1 Nogherotto-Tompkins Scheme

A new parameterization for explicit cloud microphysics and precipitation built upon the European Centre for Medium Weather Forecast's Integrated Forecast System (IFS) module (Tiedtke [1993], Tompkins [2007]), was introduced in RegCM4 (*ipptls* = 2 in *&microparam*) by Nogherotto et al. [2016]. In the present configuration, the scheme solves implicitly 5 prognostic equations for water vapor, cloud liquid water, rain, cloud ice and snow, but it is also easily extendable to a larger number of variables. Water vapor *qv*, cloud liquid water *ql*, rain *qr*, cloud ice *qi* and snow *qs* are all expressed in terms of the grid-mean mixing ratio.

Cloud liquid and ice water content are independent, allowing the existence of supercooled liquid water and mixed-phase clouds. Rain and snow precipitate with a fixed terminal fall speed and can then be advected by the three dimensional winds. A check for the conservation of enthalpy and of total moisture is ensured at the end of each timestep. The governing equation for each variable is:

$$\frac{\partial q_x}{\partial t} = S_x + \frac{1}{\rho}\frac{\partial}{\partial z}(\rho V_x q_x)$$

The local variation of the mixing ratio *qx* of the variable *x* is given by the sum of *Sx*, containing the net sources and sinks of *qx* through microphysical processes (i.e. condensation, evaporation, auto-conversion, melting, etc.), and the sedimentation term, which is a function of the fall speed *Vx* . An upstream approach is employed to solve the equations. The sources and sinks contributors are divided in two groups according to the duration of the process they describe: processes that are considered to be fast relative to the model time step are treated implicitly while slow processes are treated explicitly. The processes taken into account (shown in Figure 1) are the microphysical pathways across the 5 water variables: condensation, autoconversion, evaporation, cloud water collection (accretion), and autoconversion for warm clouds, and freezing, melting, deposition, sublimation for cold clouds.

https://doi.org/10.5194/gmd-2020-435
Preprint. Discussion started: 31 March 2021

Geoscientific Model Development Discussions
Open Access

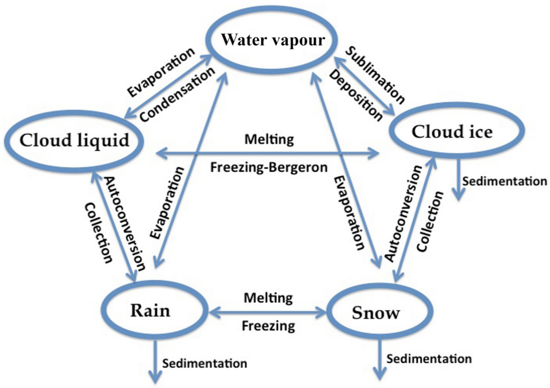

Figure 1: Depiction of the new scheme, showing the five prognostic variables and how they are related to each other through microphysical processes

For each microphysical pathway, phase changes are associated with the release or absorption of latent heat, which then impacts the temperature budget. The impact is calculated using the conservation of liquid water temperature *TL* defined as:

$$T_L = T - \frac{L_v}{C_p}(q_l + q_r) - \frac{L_s}{C_p}(q_i + q_s).$$

Given that dTL =0, the rate of change of the temperature is given by the following equation:

$$\frac{\partial T}{\partial t} = \sum_{x=1}^{m} \frac{L(x)}{C_p}\left(\frac{dq_x}{dt} - D_{q_x} - \frac{1}{\rho}\frac{\partial}{\partial z}(\rho V_x q_x)\right)$$

where *L*(*x*) is the latent heat of fusion or evaporation, depending on the process considered, *Dqx* is the convective detrainment and the third term in brackets is the sedimentation term.

At the end of each time step a check is carried out of the conservation of total water and moist static energy:

$$h = C_P T + gz + Lq_x.$$

The scheme is tunable through parameters in the *&microparam* section of the namelist (RegCM-4.7.1/Doc/README.namelist; Elguindi et al. 2017).

https://doi.org/10.5194/gmd-2020-435
Preprint. Discussion started: 31 March 2021

Geoscientific Model Development Discussions

2.1.2 WSM5 Scheme

RegCM4-NH also employs the Single-Moment 5-class microphysics scheme of the WRF model (Skamarock et al., 2008). This scheme (*ipptls* = 3 in *&microparam*) follows Hong et al. (2004) and, similarly to Nogherotto et al. (2016), includes vapor, rain, snow, cloud ice, and cloud water hydrometeors. The scheme separately treats ice and water saturation processes, assuming water hydrometeors for temperatures above freezing, and cloud ice and snow below the freezing level (Dudhia, 1989, Hong et al., 1998). It accounts for supercooled water and a gradual melting of snow below the melting layer (Hong et al., 2004, and Hong and Lim, 2006). Therefore, the WSM5 and Nogherotto-Tompkins schemes have similar structures (Figure 1), but also important differences.

Differently from the Nogherotto-Tompkins scheme, the WSM5 (as well as the other WSM schemes in WRF) prescribes an inverse exponential continuous distribution of particle size (ex. Marshall and Palmer (1948) for rain, Gunn and Marshall (1958) for snow). It also includes the size distribution of ice particles and, as a major novelty, the definition of the number of ice crystals based on ice mass content rather than temperature. Both the Nogherotto-Tompkins and WSM5 schemes include autoconversion, i.e. sub-time step processes of conversion of cloud water to rain and cloud ice to snow. For rain, Hong et al. (2004) use a Kessler (1969) type algorithm in WSM5, but with a stronger physical basis following Tripoli and Cotton (1980). The Nogherotto-Tompkins scheme also includes the original Kessler (1969) formula as an option, but it makes available other three exponential approaches following Sundqvist et al. (1989), Beheng (1994), and Khairoutdinov and Kogan (2000). For ice autoconversion the Nogherotto-Tompkins scheme uses an exponential approach (Sundqvist, 1989) with a specific coefficient for ice particles (following Lin et al., 1983) depending on temperature, while the WSM5 uses a critical value of ice mixing ratio (depending on air density) and a maximum allowed ice crystal mass (following Rutledge and Hobbs, 1983) that suppresses the process at low temperatures because of the effect of air density. Finally, the WSM5 has no dependency on cloud cover for condensation processes while the Nogherotto-Tompkins scheme uses cloud cover to regulate the condensation rate in the formation of stratiform clouds.

3 Illustrative case studies

Three case studies (Table 1) of Heavy Precipitation Events (HPE) have been identified in order to test and illustrate the behavior of the non-hydrostatic core of the RegCM4-NH, with focus on the explicit simulation of convection over different regions of the world. In two test cases, California and Lake Victoria, data from the ERA-Interim reanalysis (Dee et al. 2011) are used to provide initial and lateral meteorological boundary conditions for an intermediate resolution run (grid spacing of 12 km, with use of convection parameterizations), which then provides driving boundary conditions for the convection permitting experiments. In the Texas case study, we fed directly the fields from the ERA-Interim reanalysis to the RegCM 3km convection permitting simulation because we found that the HPE intensity was already reproduced accurately with this procedure. All simulations start 24-48 hours before the HPE.

https://doi.org/10.5194/gmd-2020-435
Preprint. Discussion started: 31 March 2021

Geoscientific Model Development Discussions
Open Access

The analysis focuses on the total accumulated precipitation over the entire model domains (Fig. 2) and the periods defined in Table 1. For the cases of California and Texas the evaluation also includes the time series of 6 hourly accumulated precipitation averaged on the region of maximum precipitation (red rectangles in Figs. 4a, b) against available high temporal resolution observations. The discussion of the case studies is presented in the next sections.

Case	**ACRONYM**	**Region of The event**	**Analyzed Time Window**
1	CAL	California	15 Feb 2004 00:00 19 Feb 2004 00:00
2	TEX	Texas	9 December 00:00 12 December 00:00
3	LKV	Lake Victoria	25 Nov 1999 00:00 1 Dec 1999 00:00

Table 1: List of acronyms of the test cases and simulation period

CAL (a)　　　　TEX (b)

https://doi.org/10.5194/gmd-2020-435
Preprint. Discussion started: 31 March 2021

Geoscientific Model Development Discussions
Open Access
EGU

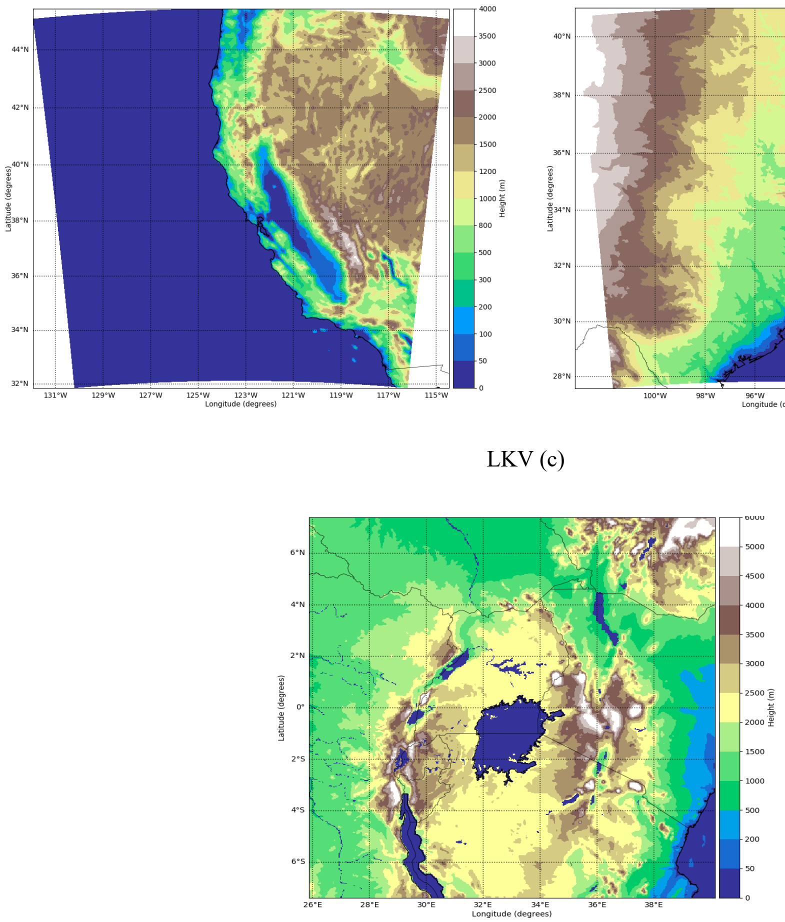

Figure 2: Domain tested , a) California (CAL) , b) Texas (TEX), c) Lake Victoria (LKV).

3.1 California

The first case, referred to as CAL (California) in Table 1, is a HPE which occurred on 16–18 February 2004, producing flooding conditions for the Russian River in coastal northern California. The event is documented in detail by *Ralph et al. (2006)*, who focused their attention on the impact of narrow filament-shaped structures of strong horizontal water vapor transport over the eastern Pacific Ocean and the western U.S. coast, called Atmospheric Rivers (ARs). ARs are typically associated with a low-level jet stream ahead of the cold front of extratropical cyclones (Zhu and Newell 1998; Dacre et al. 2015; Ralph et al. 2018), and can induce heavy precipitation where they make landfall and are forced to rise over mountain chains (Gimeno et al. 2014). The CAL event consists of a slow propagating surface front arching southeastward towards Oregon and then southwestward offshore of California (Fig.3a,c). Rain began over the

https://doi.org/10.5194/gmd-2020-435
Preprint. Discussion started: 31 March 2021

coastal mountains of the Russian River watershed at 0700 UTC, 16 February, as a warm front descended southward, and also coincided with the development of orographically favoured low-level upslope flow Ralph et al. (2006).

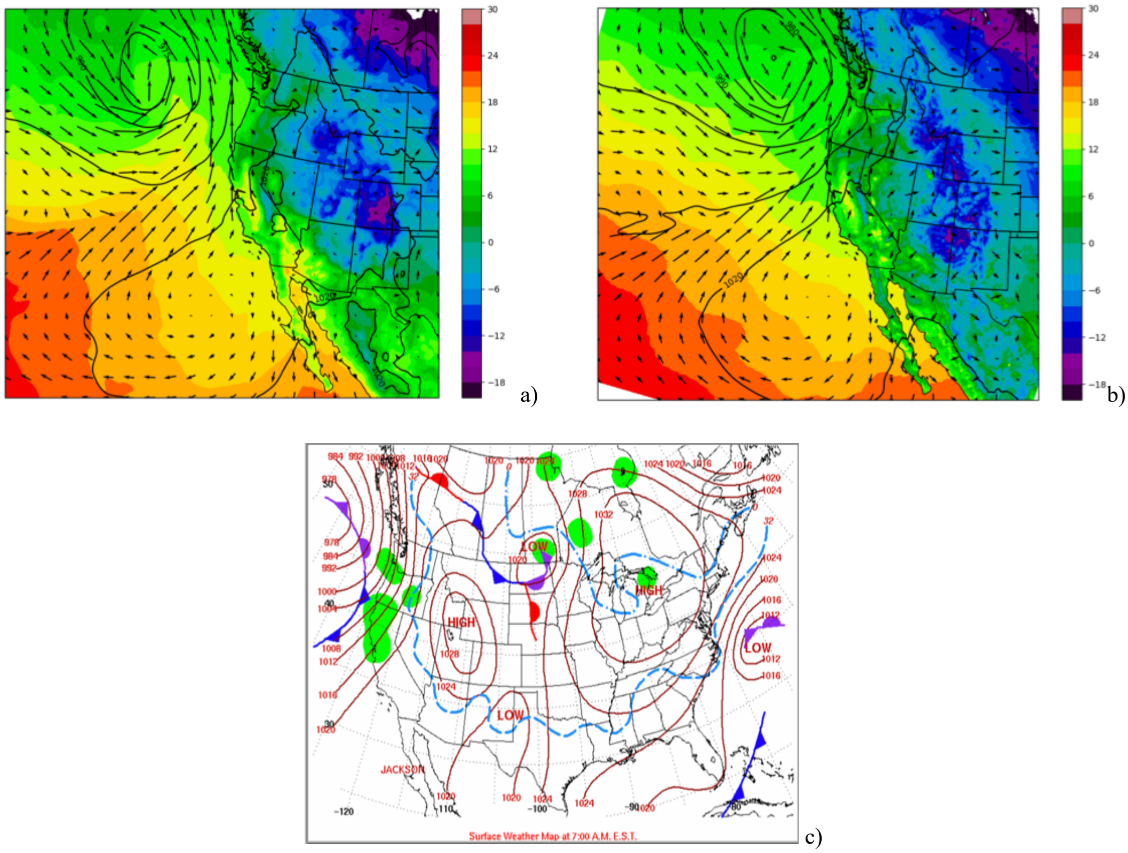

Figure 3: a,b) mean sea level pressure (mslp) (black contour lines), surface temperature (color shading) and 100-m wind direction (black arrows) at 7:00 UTC, 16 Feb. 2004 of ERA5 reanalysis and RegCM 12km respectively. c) NCEP-NOA Surface Analysis of pressure and fronts

The intermediate resolution (12 km) domain covers a wide area encompassing California and a large portion of the coastal Pacific Ocean, with 23 vertical levels and a parameterization for deep convection based on the Kain–Fritsch scheme (Kain, 2004). The ERA-Interim driven simulation is initialized at 0000 UTC, 15 February 2004 (Tab.1) and lasts until 0000 UTC 19 February 2004. This simulation drives a corresponding RegCM4-NH run using a smaller domain centered over northern California (Fig. 2a) at 3 km horizontal grid spacing and 41 vertical levels, with boundary conditions updated at 1 hour intervals. In RegCM4-NH only the shallow convection component of the Tiedtke scheme (Tiedtke,1996) is used. Simulated precipitation is validated against rainfall data from the TRMM

https://doi.org/10.5194/gmd-2020-435
Preprint. Discussion started: 31 March 2021

(0.25°x0.25°) (Huffman et al, 2007) dataset over the sea, and the CHIRPS (0.05°x0.05°) (Funk et al, 2015) dataset over the land. First, we notice that the synoptic conditions characteristic of this case study, which are fed into the RegCM4-NH model, are well reproduced by RegCM at 12 km as shown in Figure 3, where we compare the simulated mean sea level pressure (mslp), surface temperature and wind direction on 14 Feb at 7:00 am, by RegCM at 12 km (Fig.3b), with the same variables inby ERA5 (Fig.3a) and the surface analysis of pressure and fronts, derived from the operational weather maps prepared at the National Centers for Environmental Prediction, Hydrometeorological Prediction Center, National Weather Service (https://www.wpc.ncep.noaa.gov/dailywxmap/index_20040216.html) (Fig.3c).

The observed precipitation datasets place the highest maxima on the terrain elevation peaks, with extreme rainfall of greater than 250 mm in 60 hours over the coastal mountains and greater than 100 – 175 mm elsewhere in the domain (Fig. 4a). The red box in Fig.4a shows the area of the Russian River watershed, highlighting the locations of the observing systems, including Cazadero (CZD) and Bodega Bay (BBY) where the largest rainfall rates were detected respectively 269 mm and 124 mm in 60-h accumulated rainfall between 0000 UTC 16 February and 1200 UTC 18 February 2004 (Ralph et al., 2006).

The convection permitting simulation captures the basic features of the observed precipitation (Fig.4a), as shown for example in Fig.4g and 5a, both in terms of spatial distribution and temporal evolution of rainfall (Fig.5a). However, it shows higher precipitation rates than observed over the sea and over the mountain chains, with lower intensities than observed in the south-east part of the mountain chain (Fig.4g). By contrast, the 12-km simulation severely underestimates the magnitude of the precipitation event (Fig.4d).

Concerning the timing and intensity of the event in the CZD subregion, 6-hourly accumulated precipitation (Fig.5a) averaged over the red box of Figure 4a, shows that both the 3 km and 12 km simulations capture the onset of the event, but the peak intensity is strongly underestimated by the 12 km run, while it is well simulated by the 3 km run, although the secondary maximum is overestimated. Therefore, overall, our results show that only the high resolution convection permitting model captures these extreme events, and that parameterized convection has severe limits in this regard (Done et al. 2004; Lean et al. 2008; Weisman et al. 2008; Weusthoff et al. 2010; Schwartz 2014; Clark et al. 2016).

https://doi.org/10.5194/gmd-2020-435
Preprint. Discussion started: 31 March 2021

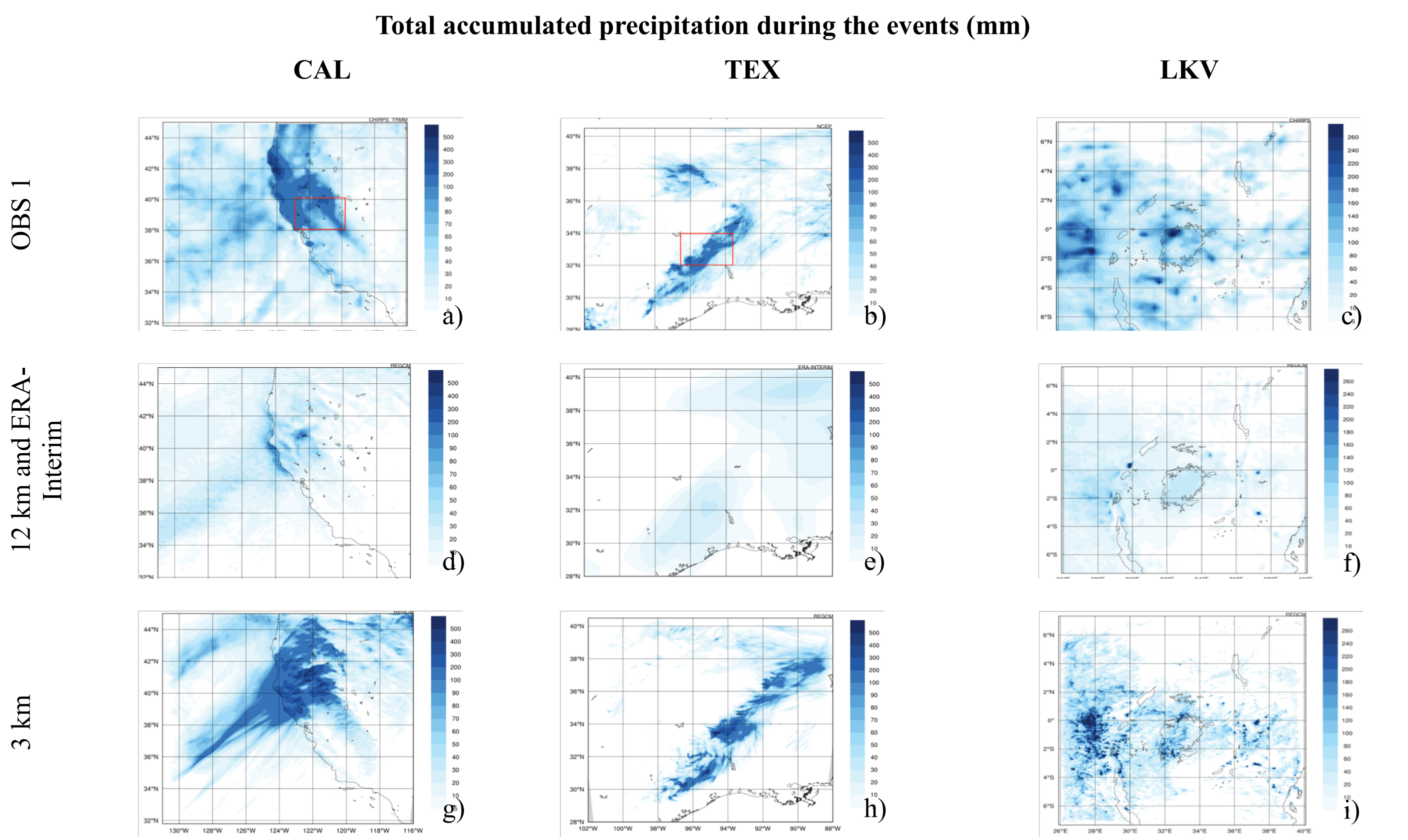

Figure 4: Total accumulated precipitation (mm) , observations: TRMM (Sea) merged with CHIRPS (Land) (a), NCEP Stage IV analysis (b), CMORPH (c). RegCM at 12 km (d,f), ERA–Interim analysis (e) and RegCM 3 km simulation (g,h,i)

https://doi.org/10.5194/gmd-2020-435
Preprint. Discussion started: 31 March 2021

CAL (a) TEX (b)

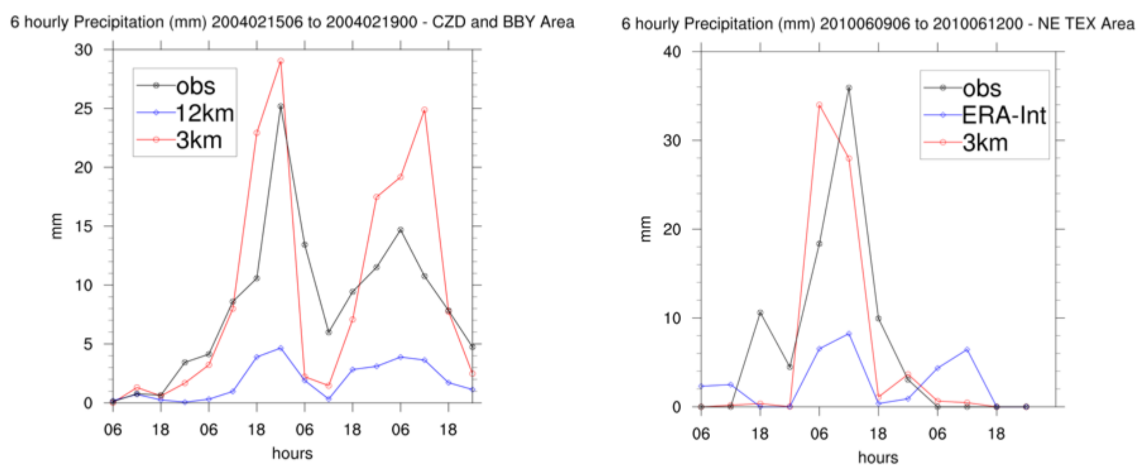

Figure 5: Time series of the 6 hourly accumulated precipitation (in mm on the y-axis) during the CAL event (a) and during the TEX event (b). The blue lines respectively shows RegCM 12 Km and ERA interim 6 hourly accumulated precipitation averaged in the area indicated by the red square in fig.2 (a,b) while the red line shows the 6 hourly accumulated precipitation simulated by RegCM 3 km. The observations are shown in black line

3.2 Texas

Case 2, hereafter referred to as TEX (Table 1), is a convective precipitation episode exhibiting characteristics of the "Maya Express" flood events, linking tropical moisture plumes from the Caribbean and Gulf of Mexico to midlatitude flooding over the central United States (Higgins 2011). During the TEX event, an upper-level cutoff low over northeastern Texas, embedded within a synoptic-scale ridge, moved slowly northeastward. Strong low-level flow and moisture transport from the western Gulf of Mexico progressed northward across eastern Texas. The event was characterized by low-level moisture convergence, weak upper-level flow, weak vertical wind shear, and relatively cold air (center of cutoff low), which favored the slow-moving convective storms and nearly stationary thunderstorm outflow boundaries. The main flooding event in eastern Texas occurred on June 10, 2010, with a daily maximum rainfall of 216.4 mm of the region in the red grid box of Figure 4b (Higgins 2011).

In the daily precipitation observations for 10 June 2010 (NCEP stage-IV gridded precipitation, Fig. 4b) the highest values related to the mesoscale convective system occur in eastern Texas (~ 200 mm), with another smaller area of maximum precipitation to the north, approximately over Oklahoma. Figures 4e and 4h show the same information as

https://doi.org/10.5194/gmd-2020-435
Preprint. Discussion started: 31 March 2021

Geoscientific Model Development
Discussions

in Figure 4b, except for Era-Interim and the RegCM4-NH, respectively. The ERA-Interim shows some of the observed features of precipitation, but it also shows a pronounced underestimation over the areas of maximum precipitation. By comparison, the RegCM4-NH simulations (Fig. 4h) show an improvement in pattern and intensity , and are substantially closer to observations over eastern Texas. However, in the non-hydrostatic simulation the precipitation area is slightly overestimated and the model is not capable of reproducing the small region of maximum precipitation in the north.

The time series of precipitation over eastern Texas from 9 to 12 June 2010 (Figure 5b) for observations (black line), ERA-Interim (blue line) and RegCM4-NH (red line) are shown in Fig.5b. Precipitation increases over this region from 00:00, 10 June, until it reaches the observed maximum at 12:00, 10 June (~35 mm), gradually decreasing afterwards until 6:00, 11 June. The RegCM4-NH simulation shows a more realistic temporal evolution than the RegCM4, which exhibits an overall underestimation. In general, the non-hydrostatic model produces precipitation values close to the observations, however, the simulated maximum is reached 6 hours earlier than observed.

3.3 Lake Victoria

Case 3 focuses on Lake Victoria (LKV), with the purpose of testing RegCM4-NH on a complex and challenging region in terms of convective rainfall. It is estimated that each year 3,000-5,000 fishermen perish on the lake due to nightly storms (Red Cross, 2014). In the Lake Victoria basin, the diurnal cycle of convection is strongly influenced by lake/land breezes driven by the thermal gradient between the lake surface and the surrounding land. As the land warms during the course of the day, a lake breeze is generated which flows from the relatively cooler water towards the warmer land surface. The circulation is effectively reversed at night, when the land surface becomes cooler than the lake surface, leading to convergence over the lake and associated thermal instability.

In the LKV region, prevailing winds are generally easterly most of the year with some variability due to the movement of the ITCZ. The local diurnal circulation created by the presence of the lake within the larger scale easterly wind field creates two diurnal rainfall maxima. During daylight hours, when the lake breeze begins to advance inland, convergence is maximized on the eastern coast of the lake as the lake breeze interacts with the prevailing easterlies. Studies have also noted the importance of downslope katabatic winds along the mountains to the east of the lake in facilitating convergence along the eastern coastal regions (Anyah et al. 2006). This creates a maximum in rainfall and convection on the eastern coast of LKV. Conversely, during nighttime hours, when the local lake circulation switches to flow from the land towards the lake, the prevailing easterlies create locally strong easterly flow across the lake and an associated maximum in convergence and rainfall on the western side of LKV.

The LKV simulation starts on 25 November 1999 and extends to the beginning of December 1999 (Table 1), covering a 5-day period which falls within the short-rain season of East Africa. The choice of 1999, an ENSO neutral year, was made in order to focus the analysis on local effects, such as the diurnal convection cycle in response to the lake/land breeze, with no influence of anomalous large scale conditions. A 1-dimensional lake model (Hostetler et al. 1993;

https://doi.org/10.5194/gmd-2020-435
Preprint. Discussion started: 31 March 2021

Geoscientific Model Development
Discussions

Bennington et al. 2014) interactively coupled to RegCM4-NH was utilized to calculate the lake surface temperature (LST), since lake-atmosphere coupling has been shown to be important for the LKV (Sun et al. 2015; Song et al. 2004). This coupled lake model has been already used for other lakes, including Lake Malawi in southern Africa (Diallo et al. 2018). As with the other experiments, the boundary conditions are provided by a corresponding 12 km RegCM4 simulation employing the convection scheme of Tiedtke (1996).

At the beginning of the simulation, the LST over the lake is uniformly set to 26C, and is then allowed to evolve according to the lake-atmosphere coupling. This initial LST value was chosen based on preliminary simulations and was shown to produce the most realistic precipitation for the period compared with CMORPH (Joyce et al, 2004). The synoptic feature favorable for the production of precipitation over the LKV in this period corresponds to a large area of southeasterly flow from the Indian Ocean (Fig. 6a). This southeasterly flow brings low-level warm moist air into the LKV region which facilitates the production of convective instability and precipitation. This synoptic setup, with a low-level south easterly jet off the Indian Ocean, is a common feature associated with high precipitation production in the LKV region (Anyah et al. 2006) is found in ERA5 (Figure 6a).

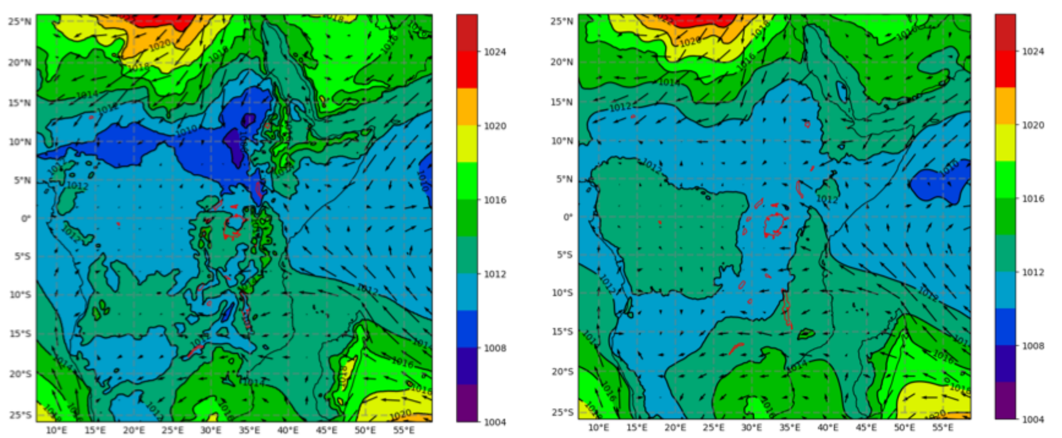

a) b)

Figure 6: mean sea level pressure (mslp) (color shading) and 100-m wind direction (black arrows) averaged over the period averaged over the period 9 December 00:00 - 12 December 00:00, of ERA5 reanalysis (a) and RegCM 12km (b). The Victoria Lake and the others lakes in the domain are highlighted in red line

The LKV region dynamics are quite distinct between nighttime and daytime and the rainfall in and around the lake has a pronounced diurnal cycle. To understand this strong diurnal cycle, Figure 7 shows a cross-section through the lake (32°E to 34°Ealong 1°S latitude at a period during strong nighttime convection (Fig. 7a; 4Z 30 November) and

https://doi.org/10.5194/gmd-2020-435
Preprint. Discussion started: 31 March 2021

during strong daytime convection (Fig. 7b; 13Z 29 November). During the day, surface heating around the lake leads to a temperature differential between the land and lake sufficient to create a lake breeze. This lake breeze is in opposition to the large scale easterly flow over the region and consequently strong convergence and convection is maximized in the highlands to the east of the lake (Fig. 7b). Conversely, during the night, the lake becomes the focus of a land breeze circulation and consequently a focus for convergence and convection as seen in Figure 7a.

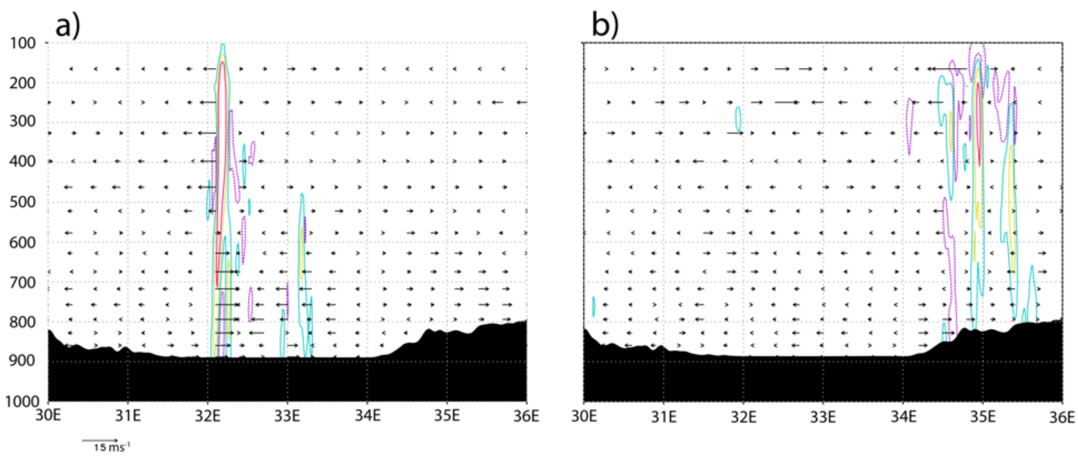

Figure 7: Cross-section through 1oS of zonal-wind anomaly (30°E-36°E) vectors and contoured vertical velocity (m/s) at a) 12Z 29 November and b) 4Z 30 November. Purple dashed contours indicate -0.5 m/s, light blue contours indicate 0.5 m/s, yellow contours indicate 2 m/s, and red contours indicate 4 m/s. Lake Victoria encompasses about 32°E to 34°E.

Figure 4c shows that the total observed rainfall for the period is characterized by diurnal rainfall maxima associated with the local lake circulation. In particular, the north-western side of the lake shows a rainfall maximum exceeding 250mm during the 5-day simulation, while most of the north-west portion of the lake shows over 150mm in total rainfall. In addition, a weaker but still significant rainfall maximum is seen on the inland south-eastern coast of LKV. Comparing the 12 km simulated rainfall (Fig. 4f) to the 3 km simulation (Fig. 4i), we find significantly less rain amounts in the former, with a wide area of rainfall around 80mm over the whole of LKV. In contrast, the 3km simulation shows significantly more localization of the rainfall patterns and this is more in agreement with the CMORPH observed totals. In particular, the 3 km simulation reproduces well the maximum in rainfall on the western side of the lake, although this is placed more along the south-west corner of the lake instead of the north-west corner. Additionally, the 12 km simulation is unable to produce the observed heavy rainfall totals in the highlands to the west of the lake region, whereas these are well captured in the 3 km simulation.

In summary, overall also this last test case indicates that the RegCM4-NH can produce realistic convective activity over this morphologically complex region, and that a significant improvement is found with respect to coarser resolution model configurations.

4 Conclusions and future outlook

In this paper we have described the development of RegCM4-NH, a non hydrostatic version of the regional model system RegCM, which was completed in response to the need of moving to simulations at convection-permitting resolutions of a few km. Towards this goal we have incorporated into the RegCM4 framework the dynamical core from the non-hydrostatic version of MM5, an approach facilitated by the fact that the RegCM system is essentially an evolution of the MM5. Some modifications to the MM5 dynamical core were also implemented to increase the model stability for long term runs, as described in section 2. RegCM4-NH also includes two explicit cloud microphysics schemes needed to describe convection and cloud processes in the absence of the use of cumulus convection schemes. Finally, we presented a few case studies of explosive convection to illustrate how the model provides realistic results in different settings and general improvements compared to the coarser resolution hydrostatic version of RegCM4 for such types of events.

RegCM4-NH is currently being used for different projects, such as the Flagship Pilot Study on convection permitting modeling (Coppola et al. 2020, Ban et al. 2021 , Pichelli et al. 2021) and the EUCP EU project (Hewitt and Lowe 2018). In these contexts, the model is being run at grid spacings of a few km for continuous decadal simulations, both driven by reanalyses of observations and GCM fields (in both cases with the use of an intermediate resolution run to act as interface) over different regions, such as the Alps, the Eastern Mediterranean, Central-Eastern Europe and the Caribbeans. This will help better validate and understand the model behavior at these high resolutions.

One of the problems of the RegCM4-NH dynamical core is that, especially for long runs with varied meteorological conditions, a relatively short time step needs to be used for stability reasons. This makes the model rather computationally demanding, although not more than other convection permitting modeling systems such as the Weather Research and Forecast model (WRF, Skamarok et al. 2008). For this reason, we are currently incorporating within the RegCM system a very different and more computationally efficient non-hydrostatic dynamical core, which will provide the basis for the next version of the model, RegCM5, to be released in the future.

Following the philosophy of the RegCM modeling system, RegCM4-NH is intended to be a public, free, open source community resource for external model users. The non-hydrostatic dynamical core has been implemented in a way that it can be activated, in place of the hydrostatic dynamics, through a user-set switch, which makes the use of RegCM4-NH particularly simple and flexible. We therefore envision that the model will be increasingly used by a broad community so that a better understanding can be achieved of its behavior, advantages and limitations.

https://doi.org/10.5194/gmd-2020-435
Preprint. Discussion started: 31 March 2021

Code Availability:

https://zenodo.org/record/4603556

https://github.com/ictp-esp/RegCM/releases/tag/4.7.1

Author contribution: CE prepared the manuscript with contributions from all co-authors and coordinated research, SP, TA, GR carried out and analysed the simulations, PE investigated solutions to stabilize/adapt the model at the km-scale and performed preliminary validation tests, GG developed/adapted the model code, FDS contributed to develop the coupled version of the model, NR developed one of the microphysics scheme, GF supervised and coordinated all activities.

Competing interests: The authors declare that they have no conflict of interest.

References

Anyah, R., Semazzi, F. H. M., Xie, L., 2006: Simulated Physical Mechanisms Associated with Climate Variability over Lake Victoria Basin in East Africa, Mon. Wea. Rev., 134 3588-3609.

Anthes, R. A., Hsie, E. -Y., & Kuo, Y. -H. (1987). *Description of the Penn State/NCAR Mesoscale Model: Version 4 (MM4)* (No. NCAR/TN-282+STR). doi:10.5065/D64B2Z90

Anyah, R. O., F. H. M. Semazzi, L. Xie, 2006: Simulated Physical Mechanisms Associated with Climate Variability over Lake Victoria Basin in East Africa. Mon. Wea. Rev., 134, 3588-3609,.

Ban, N., J. Schmidli, and C. Schär, 2014: Evaluation of the convection-resolving regional climate modeling approach in decade-long simulations. J. Geophys. Res. Atmos., 119, 7889– 7907, https://doi.org/10.1002/2014JD021478.

Ban, N., Caillaud, C., Coppola, E. et al. The first multi-model ensemble of regional climate simulations at kilometer-scale resolution, part I: evaluation of precipitation. Clim Dyn (2021). https://doi.org/10.1007/s00382-021-05708-w

Beheng, K.: A parameterization of warm cloud microphysical conversion processes, Atmos. Res., 33, 193–206, 1994

Bennington V, Notaro M, Holman KD, 2014: Improving Climate Sensitivity of Deep Lakes within a Regional Climate Model and Its Impact on Simulated Climate, J. Climl, 27, 2886-2911.

Coppola, E., Sobolowski, S., Pichelli, E. *et al.* A first-of-its-kind multi-model convection permitting ensemble for investigating convective phenomena over Europe and the Mediterranean. *Clim Dyn* 55, 3–34 (2020). https://doi.org/10.1007/s00382-018-4521-8

Chan, S. C., E. J. Kendon, H. J. Fowler, S. Blenkinsop, N. M. Roberts, and C. A. T. Ferro, 2014: The value of high-resolution Met Office regional climate models in the simula- tion of multi-hourly precipitation extremes. J. Climate, 27, 6155–6174, https://doi.org/10.1175/JCLI-D-13-00723.1.

Clark, P., N. Roberts, H. Lean, S. P. Ballard, and C. Charlton- Perez, 2016: Convection-permitting models: A step-change in rainfall forecasting. Meteor. Appl., 23, 165–181, https://doi.org/ 10.1002/met.1538.

Dacre, H. F., P. A. Clark, O. Martinez-Alvarado, M. A. Stringer, and D. A. Lavers, 2015: How do atmospheric rivers form? Bull. Amer. Meteor. Soc., 96, 1243-1255, https://doi.org/10.1175/BAMS-D-14-00031.

Dale, M., A. Hosking, E. Gill, E. J. Kendon, H. J. Fowler, S. Blenkinsop, and S. C. Chan, 2018: Understanding how changing rainfall may impact on urban drainage systems; les- sons from projects in the UK and USA. Water Pract. Technol., 13, 654–661, https://doi.org/10.2166/wpt.2018.069.

Diallo, I., Giorgi, F. and Stordal, F. (2018) Influence of Lake Malawi on regional climate from a double nested regional climate model experiment. *Climate Dynamics*, 50, 3397– 3411. https://doi.org/10.1007/s00382-017-3811-x

Dickinson, R.E., Errico, R.M., Giorgi, F. *et al.* A regional climate model for the western United States. *Climatic Change* 15, 383–422 (1989). https://doi.org/10.1007/BF00240465

Done, J., C. A. Davis, and M. L. Weisman, 2004: The next gener- ation of NWP: Explicit forecasts of convection using the Weather Research and Forecasting (WRF) model. Atmos. Sci. Lett., 5, 110–117, https://doi.org/10.1002/asl.72.

Dudhia, J., 1989: Numerical study of convection observed during the winter monsoon experiment using a mesoscale two-dimensional model, J. Atmos. Sci., 46, 3077–3107.

Durran D.R. and Klemp J.B.: A compressible model for the simulation of moist mountain waves, Mon. Wea. Rev., 111, 2341–236, 1983.

Elguindi N., Bi X., Giorgi F. , Nagarajan, B. Pal J., Solmon F., Rauscher S., Zakey S., O'Brien T., Nogherotto R. and Giuliani G., 2017: Regional Climate Model RegCMReference ManualVersion 4.7, 49 pp, https://zenodo.org/record/4603616

Funk, C., Peterson, P., Landsfeld, M. *et al.* The climate hazards infrared precipitation with stations—a new environmental record for monitoring extremes. *Sci Data* 2, 150066 (2015). https://doi.org/10.1038/sdata.2015.66

Gimeno, L., R. Nieto, M. Vàsquez, and D. A. Lavers, 2014: Atmospheric rivers: A mini-review. Front. Earth Sci., 2, https://doi.org/10.3389/feart.2014.00002.

Giorgi F (2019) Thirty years of regional climate modeling: where are we and where are we going next? J Geophys Res Atmos 124:5696–5723

https://doi.org/10.5194/gmd-2020-435
Preprint. Discussion started: 31 March 2021

Geoscientific Model Development Discussions
Open Access
EGU

Giorgi F et al (2012) RegCM4: model description and preliminary tests over multiple CORDEX domains. Clim Res 52:7–29

Giorgi F, Jones C, Asrar G (2009) Addressing climate information needs at the regional level: the CORDEX framework. WMO Bull 175–183

Giorgi F, Mearns LO (1999) Introduction to special section: regional climate modeling revisited. J Geophys Res 104:6335–6352

Giorgi F, Marinucci MR, Bates G, DeCanio G (1993b) Development of a second generation regional climate model (RegCM2), part II: convective processes and assimilation of lateral boundary conditions. Mon Weather Rev 121:2814–2832

Giorgi, F., and G. T. Bates, 1989: The Climatological Skill of a Regional Model over Complex Terrain. *Mon. Wea. Rev.*, **117**, 2325–2347, https://doi.org/10.1175/1520-0493(1989)117<2325:TCSOAR>2.0.CO;2.

G. A. Grell, J. Dudhia and D. R. Stauffer, “A Description of the Fifth Generation Penn State/NCAR Mesoscale Model (MM5),” NCAR Tech. Note, NCAR/TN-398+ STR, Boulder, 1995, p. 122.

Gunn, K. L. S., and J. S. Marshall, 1958: The distribution with size of aggregate snowflakes. J. Meteor., 15, 452–461, https://doi.org/10.1175/1520-0469(1958)015<0452:TDWSOA>2.0.CO;2.

Gutowski Jr., W. J., Giorgi, F., Timbal, B., Frigon, A., Jacob, D., Kang, H.-S., Raghavan, K., Lee, B., Lennard, C., Nikulin, G., O'Rourke, E., Rixen, M., Solman, S., Stephenson, T., and Tangang, F.: WCRP COordinated Regional Downscaling EXperiment (CORDEX): a diagnostic MIP for CMIP6, Geosci. Model Dev., 9, 4087–4095, https://doi.org/10.5194/gmd-9-4087-2016, 2016

Huffman, G. J., and Coauthors, 2007: The TRMM Multisatellite Precipitation Analysis (TMPA): Quasi-global, multiyear, combined-sensor precipitation estimates at fine scales. *J. Hydrometeor.*, **8**, 38–55, doi:https://doi.org/10.1175/JHM560.1

Lean, H. W., P. A. Clark, M. Dixon, N. M. Roberts, A. Fitch, R. Forbes, and C. Halliwell, 2008: Characteristics of high- resolution versions of the Met Office Unified Model for forecasting convection over the United Kingdom. Mon. Wea. Rev., 136, 3408–3424, https://doi.org/10.1175/2008MWR2332.1.

https://doi.org/10.5194/gmd-2020-435
Preprint. Discussion started: 31 March 2021

Geoscientific Model Development Discussions
Open Access
EGU

Lind, P., D. Lindstedt, E. Kjellstrom, and C. Jones, 2016: Spatial and temporal characteristics of summer precipitation over central Europe in a suite of high-resolution climate models. J. Climate, 29, 3501–3518, https://doi.org/10.1175/JCLI-D-15- 0463.1.

Hewitt, C. D., and J. A. Lowe, 2018: Toward a European climate prediction system. Bull. Amer. Meteor. Soc., 99, 1997–2001, https://doi.org/10.1175/BAMS-D-18-0022.1.

Hong, S.-Y., H.-M. H. Juang, and Q. Zhao, 1998: Implementation of prognostic cloud scheme for a regional spectral model, Mon. Wea. Rev., 126, 2621–2639.

Hong, S.-Y., J. Dudhia, and S.-H. Chen, 2004: A Revised Approach to Ice Microphysical Processes for the Bulk Parameterization of Clouds and Precipitation, Mon. Wea. Rev., 132, 103–120.

Hong, S.-Y., and J.-O. J. Lim, 2006: The WRF Single-Moment 6-Class Microphysics Scheme (WSM6), J. Korean Meteor. Soc., 42, 129–151

Hostetler SW, Bates GT, Giorgi F, 1993: Interactive Coupling of Lake Thermal Model with a Regional climate Model, J. Geophys. Res., 98(D3), 5045-5057.

Joyce, Robert J., John E. Janowiak, Phillip A. Arkin, Pingping Xie, 2004: CMORPH: A Method that Produces Global Precipitation Estimates from Passive Microwave and Infrared Data at High Spatial and Temporal Resolution. J. Hydrometeor, 5, 487–503

Kain, J. S., 2004: The Kain–Fritsch convective parameterization: An update. J. Appl. Meteor., 43, 170–181, https://doi.org/10.1175/1520-0450(2004)043<0170:TKCPAU>2.0.CO;2.

Kendon, E. J., N. M. Roberts, C. A. Senior, and M. J. Roberts, 2012: Realism of rainfall in a very high-resolution regional climate model. J. Climate, 25, 5791–5806, https://doi.org/ 10.1175/JCLI-D-11-00562.1.

Kendon, E. J., and Coauthors, 2017: Do convection-permitting regional climate models improve projections of future precipitation change? Bull. Amer. Meteor. Soc., 98, 79–93, https://doi.org/ 10.1175/BAMS-D-15-0004.1

Kessler, E., 1969: On the Distribution and Continuity of Water Substance in Atmospheric Circulations. Meteor. Monogr., No. 32, Amer. Meteor. Soc., 84 pp.

Khairoutdinov, M. and Kogan, Y.: A new cloud physics parameterization in a large-eddy simulation model of marine stratocumulus, B. Am. Meteorol. Soc., 128, 229–243, 2000

Klemp, J.B. and Dudhia, J.: An Upper Gravity-Wave Absorbing Layer for NWP Applications, Monthly Weather Review, 176, 3987-4004, 2008.

Klemp, J. B. and D. K. Lilly: Numerical simulation of hydrostatic mountain waves, J. Atmos. Sci., 35, 78–107, 1978.

Lin, Y., Farley, R., and Orville, H.: Bulk parameterization of the snow field in a cloud model, J. Appl. Meteor. Clim., 22, 1065–1092, 1983.

Marshall, J. S., and W. McK. Palmer, 1948: The distribution of raindrops with size. J. Meteor., 5, 165–166.

Nogherotto, R., Tompkins, A.M., Giuliani, G., Coppola, E. and Giorgi, F.: Numerical framework and performance of the new multiple-phase cloud microphysics scheme in RegCM4. 5: precipitation, cloud microphysics, and cloud radiative effects. *Geoscientific Model Development*, *9*(7), 2533-2547, 2016

Pal JS et al (2007) The ICTP RegCM3 and RegCNET: regional climate modeling for the developing world. Bull Am Meteorol Soc 88:1395–1409

Pichelli, E., Coppola, E., Sobolowski, S. et al. The first multi-model ensemble of regional climate simulations at kilometer-scale resolution part 2: historical and future simulations of precipitation. Clim Dyn (2021). https://doi.org/10.1007/s00382-021-05657-4

Prein, A. F. et al. A review on regional convection-permitting climate modeling: demonstrations, prospects, and challenges. *Rev. Geophys.* 53, 323–361 (2015).

Ralph, F. M., P. J.Neiman, G. A.Wick, S. I.Gutman, M. D.Dettinger, D. R.Cayan, and A. B.White, 2006: Flooding on California's Russian River: Role of atmospheric rivers. *Geophys. Res. Lett.*, **33**, L13801, https://doi.org/10.1029/2006GL026689

Ralph, F. M., M. D. Dettinger, M. M. Cairns, T. J. Galarneau, and J. Eylander, 2018: Defining "atmospheric river": How the Glossary of Meteorology helped resolve a debate. Bull. Amer. Meteor. Soc., 99, 837–839, https://doi.org/10.1175/BAMS-D-17-0157.1

Rutledge, S. A., and P. V. Hobbs, 1983: The mesoscale and microscale structure and organization of clouds and precipitation in midlatitude cyclones. Part VIII: A model for the ''seeder-feeder'' process in warm-frontal rainbands. J. Atmos. Sci., 40, 1185–1206.

https://doi.org/10.5194/gmd-2020-435
Preprint. Discussion started: 31 March 2021

Geoscientific Model Development Discussions
Open Access

Skamarock WC, Klemp JB, Dudhia J, Gill DO, Barker DM, Duda MG, Huang XY, Wang W, Powers JG. 2008. 'A description of the advanced research WRF version 3', Technical Note NCAR/TN-475+STR. NCAR: Boulder, CO

Schwartz, C. S., 2014: Reproducing the September 2013 record- breaking rainfall over the Colorado Front Range with high- resolution WRF forecasts. Wea. Forecasting, 29, 393–402, https://doi.org/10.1175/WAF-D-13-00136.1

Sitz, L. E., F. Sante, R. Farneti, R. Fuentes-Franco, E. Coppola, L. Mariotti, M. Reale, et al. 2017. "Description and Evaluation of the Earth System Regional Climate Model (RegCM–ES)." *Journal of Advances in Modeling Earth Systems*. doi:10.1002/2017MS000933

Song Y, Semazzi HMF, Xie L, Ogallo LJ, 2004: A coupled regional climate model for the Lake Victoria Basin of East Africa. Int. J. Climatol. 24: 57-75.

Sun X, Xie L, Semazzi F, Liu B, 2015: Effect of Lake Surface Temperature on the Spatial Distribution and Intensity of the Precipitation over the Lake Victoria Basin. Mon. Wea. Rev. 143: 1179-1192.

Sundqvist, H., Berge, E., and Kristjansson, J.: Condensation and cloud parameterization studies with a mesoscale numerical weather prediction model, Mon. Weather Rev., 117, 1641–1657,1989.

Tiedtke, M., . 1996: An extension of cloud-radiation parameterization in the ECMWF model: The representation of subgrid-scale variations of optical depth.Mon. Wea. Rev., 124, 745–750

Tiedtke, M., 1993: Representation of Clouds in Large-Scale Models. Mon. Wea. Rev., 121, 3040–3061, https://doi.org/10.1175/1520-0493(1993)121<3040:ROCILS>2.0.CO;2

Tompkins, A.: Ice supersaturation in the ECMWF integrated fore-cast system, Q. J. Roy. Meteor. Soc., 133, 53–63, 2007

Tripoli, G. J., and W. R. Cotton, 1980: A numerical investigation of several factors contributing to the observed variable intensity of deep convection over south Florida. J. Appl. Meteor., 19, 1037–1063.

Williams PD. 2009. A proposed modification to the Robert–Asselin time filter. Mon. Weather Rev. 137: 2538–2546

Weisman, M. L., C. Davis, W. Wang, K. W. Manning, and J. B. Klemp, 2008: Experiences with 0–36-h explicit convective forecasts with the WRF-ARW model. Wea. Forecasting, 23, 407–437, https://doi.org/10.1175/2007WAF2007005.1

https://doi.org/10.5194/gmd-2020-435
Preprint. Discussion started: 31 March 2021

Geoscientific Model Development Discussions

Weusthoff, T., F. Ament, M. Arpagaus, and M. W. Rotach, 2010: Assessing the benefits of convection-permitting models by neigh- borhood vertification: Examples from MAP D-PHASE. Mon. Wea. Rev., 138, 3418–3433, https://doi.org/10.1175/2010MWR3380.1.

Zhu, Y., and R. E. Newell, 1998: A proposed algorithm for moisture fluxes from atmospheric rivers. Mon. Wea. Rev., 126, 725–735, https://doi.org/10.1175/1520- 0493(1998)126<0725:APAFMF>2.0.CO;2.